Polarization switching and injection locking in vertical-cavity surface-emitting lasers subject to parallel optical injection

Quirce, Ana; Perez, Pablo; Popp, Alexandra; Valle, A.; Pesquera, Luis; Hong, Yanhua; Thienpont, Hugo; Panayotov, Krassimir

Published in:
Opt. Lett.

DOI:
10.1364/OL.41.002664

Publication date:
2016

Optics Letters

Polarization switching and injection locking in vertical-cavity surface-emitting lasers subject to parallel optical injection

Ana Quirce,[1,*] Pablo Pérez,[2] Alexandra Popp,[2] Ángel Valle,[2] Luis Pesquera,[2] Yanhua Hong,[3] Hugo Thienpont,[1] and Krassimir Panajotov[1,4]

[1]Vrije Universiteit Brussel, Faculty of Engineering Sciences, Brussels Photonics Team B-PHOT, Pleinlaan 2, 1050 Brussels, Belgium
[2]Instituto de Física de Cantabria, Consejo Superior de Investigaciones Científicas (CSIC), Universidad de Cantabria, 39005 Santander, Spain
[3]School of Electronic Engineering, Bangor University, Gwynedd LL57 1UT, Wales, UK
[4]Institute of Solid State Physics, 72 Tzarigradsko, Chaussee Blvd., 1784 Sofia, Bulgaria
*Corresponding author: aquirce@b-phot.org

Received 22 April 2016; accepted 29 April 2016; posted 6 May 2016 (Doc. ID 263842); published 1 June 2016

Polarization switching in a long-wavelength vertical-cavity surface-emitting laser (VCSEL) under parallel optical injection is analyzed in a theoretical and experimental way. For the first time, to our knowledge, we report experimentally a state in which injection locking of the parallel polarization and excitation of the free-running orthogonal polarization of the VCSEL are simultaneously obtained. We obtain very simple analytical expressions that describe both linear polarizations. We show that the power of both linear polarizations depend linearly on the injected power in such a way that the total power emitted by the VCSEL is constant. We perform a linear stability analysis of this solution to characterize the region of parameters in which it can be observed. Our measurements qualitatively confirm the previous theoretical predictions.

OCIS codes: (140.3520) Lasers, injection-locked; (140.5960) Semiconductor lasers; (140.7260) Vertical cavity surface emitting lasers.

http://dx.doi.org/10.1364/OL.41.002664

Polarization switching (PS) and the underlying physical mechanisms in vertical-cavity surface-emitting lasers (VCSELs) subject to optical injection have attracted considerable attention in recent years [1,2]. PS in VCSELs has been usually obtained for the case of orthogonal optical injection: linearly polarized light from an external laser is injected orthogonally to the linear polarization of the solitary VCSEL. Just a few experimental works have shown that PS can also be obtained for parallel optical injection, that is, the directions of linear polarization of the injected light and the free-running VCSEL are parallel [1,3].

Parallel optical injection in Fabry–Perot cavity semiconductor lasers has been extensively studied [4–8]. Most of the studies have focused on single-mode semiconductor lasers [4–9]. Only very recently an analytical study of an optically injected two-polarization modes semiconductor laser has shown that pure- and mixed-mode steady states can coexist [10]. Linear stability analysis has been performed to highlight conditions for bistability between pure- and mixed-mode steady states [10].

In this work we obtain, experimentally and theoretically, PS in a single mode VCSEL subject to parallel optical injection around the frequency of the parallel polarization mode of the free running VCSEL. We describe a novel situation in which injection locked emission in the parallel polarization and excitation of the free-running orthogonal polarization of the VCSEL occur simultaneously. This is an unusual situation because optical injection in the polarization with smaller optical losses causes emission in the polarization with larger losses. We show that in this regime, very simple analytical expressions describing the power and phase of both linear polarization modes can be derived. A linear stability analysis using the results of Ref. [10] is performed to characterize the values of injected power and frequency detuning in which the new solution is observed. Our theoretical results are experimentally verified.

The parallel optical injection is achieved using the all-fiber experimental setup shown in [11]. The light from a tunable laser (master laser) is injected into a commercial 1550-nm VCSEL (RayCan) via a three-port optical circulator. The first polarization controller (PC1) is adjusted to assure the parallel optical injection configuration.

A second polarization controller is connected to a polarization beam splitter (PBS) to select the parallel and the orthogonal polarizations, which are analyzed by the power meters (PM) or by a high-resolution, 10 MHz, optical spectrum analyzer (BOSA). Injected power is characterized by using a 50/50 coupler instead of the 90/10 coupler of [11] and another PM.

Our VCSEL operates in a single transverse mode regime with a threshold current of 1.66 mA at 298 K. The temperature and the bias current of the VCSEL are held constant at 298 K and $I_{\mathrm{VCSEL}} = 3.05$ mA, respectively. The free-running VCSEL emits in a linear polarization that we will call the

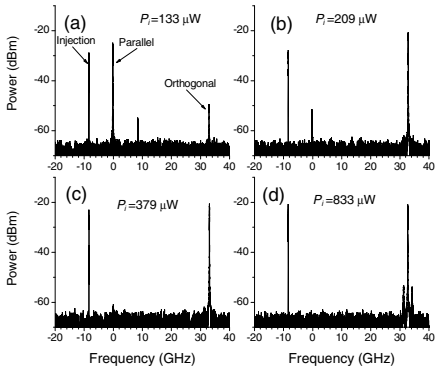

Fig. 1. Experimental optical spectra of the total output power when $\nu_i = -8.4$ GHz for different injected powers (a) $P_i = 133$ μW, (b) $P_i = 209$ μW, (c) $P_i = 379$ μW, and (d) $P_i = 833$ μW.

"parallel" (or x) polarization at the wavelength $\lambda_x = 1540.91$ nm. The orthogonal (y) polarization (34 dB weaker than the parallel polarization) is shifted by 0.26 nm toward the short wavelength side ($\lambda_y = 1540.65$ nm); the birefringence of the VCSEL is then 33 GHz. We characterize the optical injection by its strength given by the value of the power measured in front of the VCSEL, P_i, and by the frequency detuning, ν_i, defined by the difference between the injected frequency and the frequency of the free-running VCSEL.

Figure 1 shows the experimental optical spectra of the total power as P_i is increased for a fixed value of the frequency detuning, $\nu_i = -8.4$ GHz. The zero value of the frequency in the optical spectra has been chosen to correspond to the parallel polarization of the free-running VCSEL. The observed signal is the coherent addition of the VCSEL emission and the reflection of the optical injection from the front surface of the VCSEL. Figure 1(a) shows that parallel polarization mode experiences period-one dynamics with a frequency equal to the frequency detuning ν_i. Figure 1(b) shows that when P_i increases, PS is obtained: the orthogonal (parallel) polarization is excited (suppressed) at its free-running frequency. PS is maintained over a wide range of P_i [see also Figs. 1(c) and 1(d)]. Figure 1(c) demonstrates injection locked emission in the parallel polarization with a simultaneous excitation of the free-running orthogonal polarization mode of the VCSEL. We will term this situation as IL + PS. Figure 1(c) also shows that the light emitted in the parallel direction at the free-running frequency decreases as P_i increases. As we increase P_i further, the orthogonally polarized emission shows two satellite peaks around the central peak [see Fig. 1(d)]. The frequency separation between the main and the satellite peaks is 1.45 GHz, which is slightly below the relaxation oscillation frequency value, 2 GHz. For $P_i > 900$ μW injection locking in the parallel polarization without lasing of the orthogonal polarization (not shown) is obtained.

In order to explain these findings, we consider a rate equation model for the polarization modes of a single-mode VCSEL based on the spin-flip model (SFM) [12], in which we introduce an injection term (to account for a linearly polarized optical injection in the direction of emission of the solitary VCSEL). We use the parameters that were extracted for a similar free-running VCSEL in a previous work [13]. The model equations are given in [14] modified to consider a single parallel optical injection without fluctuations in the phase, where $E_{x,y}$ are the two linearly polarized slowly varying components of the field in the x and y directions, and D and n are two carrier variables. D accounts for the total population inversion between conduction and valence bands, while n is the difference between the population inversions for the spin-up and spin-down radiation channels. The model parameters are the following: the field decay rate ($\kappa = 33$ ns^{-1}), the linear dichroism ($\gamma_a = -0.1$ ns^{-1}), the linewidth enhancement factor ($\alpha = 2.8$), the linear birefringence ($\gamma_p = 103.34$ ns^{-1}), the decay rate of D ($\gamma = 2.08$ ns^{-1}), the spin-flip relaxation rate ($\gamma_s = 2100$ ns^{-1}), and the normalized bias current ($\mu = 2.29$) that corresponds to 3.05 mA. E_{inj} is the amplitude of the injected light. ν_{inj} is the detuning between the frequency of the injected light and the intermediate frequency between those of the x and y polarization, ν_x and ν_y, where $2\pi\nu_x = \alpha\gamma_a - \gamma_p$ and $2\pi\nu_y = \gamma_p - \alpha\gamma_a$, and therefore $\nu_i = \nu_{\text{inj}} - \nu_x$.

Figure 2 shows the theoretical optical spectra obtained for several values of E_{inj} when $\nu_i = -8.4$ GHz, similarly to Fig. 1. The optical spectrum corresponding to each linear polarization is plotted with a different color. The behavior is qualitative similar to that shown in Fig. 1: PS is obtained when increasing E_{inj}, as it is shown in Figs. 2(a) and 2(b). A small peak in the parallel emission at the free-running frequency appears in Figs. 2(c) and 2(d). This peak disappears when neglecting spontaneous emission noise (not shown). This indicates that IL + PS solution is also obtained in the theory. The frequency separation between the main and the satellite peaks that appear for the orthogonal polarization in Fig. 2(d) is 1.8 GHz, that is, slightly below the theoretical relaxation oscillation frequency $= (2\kappa\gamma(\mu - 1))^{1/2}/2\pi = 2.1$ GHz. Also, as in the experiment, for values of E_{inj} slightly larger than those of Fig. 2(d), ($E_{\text{inj}} > 1$) injection locking in the parallel direction without lasing of the orthogonal polarization is obtained.

A simple analysis of the IL + PS solution can be performed because the spin-flip relaxation rate is very large and therefore n is very small [13]. If we make the approximation $n = 0$ in the Eqs. (1)–(4) in [14] and write $E_x(t) = A_x(t)\exp(i(2\pi\nu_{\text{inj}}t + \phi_x(t))$, $E_y(t) = A_y(t)\exp(i(2\pi\nu_y t + \phi_y(t))$, we obtain

$$\dot{A}_x = (\kappa(D - 1) - \gamma_a)A_x + \kappa E_{\text{inj}}\cos\phi_x, \quad \textbf{(1)}$$

$$\dot{A}_y = (\kappa(D - 1) + \gamma_a)A_y, \quad \textbf{(2)}$$

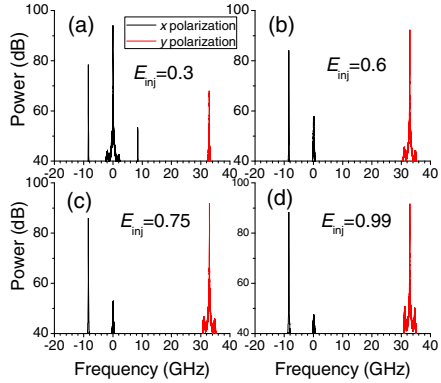

Fig. 2. Theoretical optical spectra when $\nu_i = -8.4$ GHz for different values of E_{inj}. Black (red) color represents the parallel (orthogonal) polarization.

$$\dot{\phi}_x = \kappa\alpha(D-1) - 2\pi\nu_i - \alpha\gamma_a - \kappa E_{\text{inj}} \sin\phi_x/A_x, \quad (3)$$

$$\dot{\phi}_y = \alpha(\kappa(D-1) + \gamma_a), \quad (4)$$

$$\dot{D} = -\gamma[D(1 + A_x^2 + A_y^2) - \mu]. \quad (5)$$

If we look for the steady-state solution with $A_x > 0$, and $A_y > 0$ that characterizes the IL + PS solution we obtain from Eq. (2), that $D = 1 - \gamma_a/\kappa$, that is, the total population inversion is fixed to a value that does not depend on A_x nor ϕ_x. In this way, the fact that the depressed polarization mode is lasing provides a simple expression for carrier density D. Notice that when a single-polarization mode is considered, the carrier density is given by $D = 1 + \gamma_a/\kappa - E_{\text{inj}}\cos(\phi_x)/A_x$, where A_x is found solving a third-order equation also involving ϕ_x. Steady-state values can be found by making the temporal derivatives in Eqs. (1), (3), and (5) equal to zero and substituting $D = 1 - \gamma_a/\kappa$. We obtain $\sin\phi_x = -2\gamma_a(\pi\nu_i/\gamma_a + \alpha)A_x/(\kappa E_{\text{inj}})$, $\cos\phi_x = 2\gamma_a A_x/(\kappa E_{\text{inj}})$, $A_x^2 + A_y^2 = \mu/(1 - \gamma_a/\kappa) - 1$. After some operations we obtain:

$$P_x = \left(\frac{\kappa}{2\gamma_a}\right)^2 \frac{P_{\text{inj}}}{1 + \left(\frac{\pi\nu_i}{\gamma_a} + \alpha\right)^2}, \quad (6)$$

$$P_y = \frac{\mu}{1 - \gamma_a/\kappa} - 1 - P_x, \quad (7)$$

$$\phi_x = -\arctan\left(\frac{\pi\nu_i}{\gamma_a} + \alpha\right), \quad (8)$$

where $P_{\text{inj}} = E_{\text{inj}}^2$, $P_x = A_x^2$, and $P_y = A_y^2$ are the power of the optical injection, x and y polarizations, respectively. Equations (6) and (7) show that in the IL + PS solution both P_x and P_y depend linearly on P_{inj} in such a way that the total power is constant.

We can check these predictions by measuring the power in the x, $\mathbf{P_x}$, and y, $\mathbf{P_y}$, polarizations as a function of P_i. $\mathbf{P_x}$ is obtained from the power measured at the parallel PBS output, $\mathbf{P_{par}}$, that includes the contributions of both the light emitted by the VCSEL in the parallel polarization and the reflection at the VCSEL mirror of the injected light. Equation (8) shows that the phase difference between these two fields is very close to 90°. Therefore $\mathbf{P_x} = \mathbf{P_{par}} - \mathbf{P_{ref}}$, where $\mathbf{P_{ref}}$ is the reflected power, that is the power measured at the parallel port of the PBS when the VCSEL is off.

Figure 3 shows $\mathbf{P_{par}}$, $\mathbf{P_x}$, $\mathbf{P_y}$, and the total power ($\mathbf{P_{tot}} = \mathbf{P_x} + \mathbf{P_y}$) as a function of P_i when $\nu_i = -8.6$ GHz.

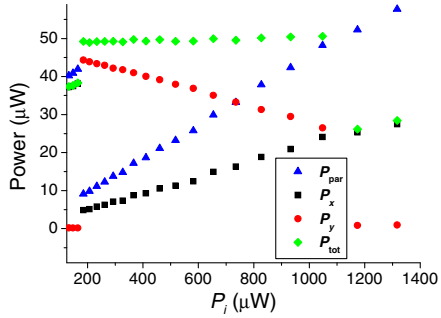

Fig. 3. Experimental values of the power at the parallel port of PBS (P_{par}), of x-polarization (P_x), of y-polarization (P_y) and of the total power (P_{tot}) as a function of P_i when $\nu_i = -8.6$ GHz.

PS is observed when 175 μW $< P_i <$ 1045 μW. In this range the IL + PS solution is observed. $\mathbf{P_x}$ and $\mathbf{P_y}$ depend linearly on P_i, in agreement with Eqs. (6) and (7): $\mathbf{P_x}$ and $\mathbf{P_y}$ are well fitted to straight lines, $\mathbf{P_x} = 0.021P_i + 0.594$ μW ($R^2 = 0.996$), and $\mathbf{P_y} = -0.02P_i + 48.338$ μW ($R^2 = 0.998$). $\mathbf{P_{tot}}$ is almost constant; it changes just a 3% from $P_i =$ 175 μW to $P_i =$ 1045 μW, in agreement with Eq. (7).

We have also characterized the region of parameters space in which the IL + PS solution is observed. Experimentally, for a fixed value of ν_i, we increase P_i from zero and record the range of P_i in which IL + PS is observed in the optical spectrum. This process is repeated for several values of ν_i. The results are shown in Fig. 4(a) for $I_{\text{VCSEL}} = 3.05$ mA. A new region in which IL + PS is observed appears at positive values of ν_i. This region appears at lower values of P_i than those observed at negative values of ν_i.

We have also analyzed the linear stability properties of our VCSEL using the analytical results obtained very recently in Ref. [10]. Our initial rate in [14] are not similar to those for the transverse electric (TE) and transverse magnetic (TM) modes of Ref. [10]. However, our Eqs. (1)–(5), based on the large value of our VCSEL spin-flip rate, are mathematically equivalent to the case of TE injection in Ref. [10] and the analytical expressions for the stability analysis of the TE + TM steady-state solution derived in that reference can be used in our case. Figure 4(b) shows the Hopf bifurcations from the two-mode steady state that are obtained by using the expressions of Ref. [10] with our VCSEL parameters. Within these two regions, at positive and negative ν_i, the TE + TM steady state, that is the IL + PS state, is stable. Comparison between Figs. 4(a) and 4(b) shows that good qualitative agreement is found between experiments and theory.

The theory developed in Ref. [10] can help to explain why the IL + PS solution appears when the VCSEL is subject to parallel optical injection. The parameter that measures the losses of the y polarization compared to the losses of the x polarization, β, [10] is positive for our VCSEL parameters ($\beta = 0.003$). The parameter β_c that gives the upper bound for the presence of a stable mixed-mode solution [10] is 0.034 in our case. Therefore, the condition, $\beta < \beta_c$, [10] for which an unsupported polarization mode (y) may be activated by injecting light into the natural supported mode (x) holds for our experiment.

Bistability between the injection locked (single-mode) and a two-color equilibrium state (steady state) has been observed in a two-color laser [15]. We observe theoretically and experimentally bistability between the IL + PS and the x-polarized

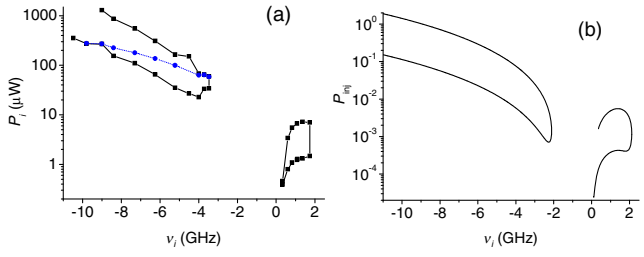

Fig. 4. (a) Experimental and (b) theoretical values of injected power for which IL + PS is observed as a function of ν_i, for $I_{\text{VCSEL}} = 3.05$ mA. The dashed line in (a) marks the lower boundary of the bistable region.

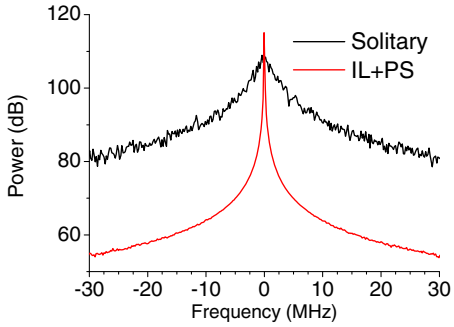

Fig. 5. Theoretical optical spectra of the power for the solitary VCSEL (black) and when $\nu_i = -8.4$ GHz and $E_{\text{inj}} = 0.9$ (red).

injection locked solutions. The region of space parameters in which bistable behavior is observed is shown in Fig. 4(a). It corresponds to the region above the dashed line and below the upper boundary of the IL + PS region. Optically bistable semiconductor lasers have applications in all-optical signal processing, including optical memory, flip-flop or optical logic [14]. One of the advantages of our bistable behavior is that the phase noise in the IL + PS state is substantially reduced with respect to the solitary VCSEL case due to the injection locked behavior of the x-polarized light. Figure 5 shows that linewidth of the x-polarization in the IL + PS state is much smaller than the one corresponding to the solitary VCSEL. In Fig. 5 the optical spectrum for IL + PS has been shifted 8.4 GHz to the right in order to compare both spectra.

Our approximate Eqs. (1)–(5) are based on the large value of the spin-flip relaxation rate measured for a similar device [13]. In order to see if our approximation is reasonable, we have used the initial SFM [14] to obtain the range of variation of the n variable in the IL + PS state. We obtain that n oscillates around the zero value with $\nu_y - \nu_{\text{inj}}$ frequency but with a very small amplitude [$9\ 10^{-4}$ for the case illustrated in Fig. 2(c)]. This small amplitude value justifies our approximation.

The IL + PS state is unusual because of the following reasons. Our free-running VCSEL is emitting in the x – linear polarization because $\gamma_a < 0$. In this way, the steady-state total population inversion is $D_x = 1 + \gamma_a/\kappa < 1$. The corresponding population inversion for the solitary device to emit in the y-linear polarization is $D_y = 1 - \gamma_a/\kappa > 1$. Under the usual conditions for an injection locked single-mode laser diode, the steady state population inversion is $D = 1 + \gamma_a/\kappa - E_{\text{inj}} \cos(\phi_x)/A_x$. In this way, D decreases when the injected field, E_{inj}, increases and therefore D can not reach D_y because $D < 1$. However, when considering a two polarization modes VCSEL below the IL + PS region of Fig. 4(a) [like for instance in Fig. 1(a)], period-1 dynamics is observed in such a way that D oscillates with a frequency given by ν_i. The amplitude of these oscillations increases as the injected power increases. In this way, as the system gets closer to the IL + PS region, D oscillates, reaching values well above D_y. The two-mode solution with $D = 1 - \gamma_a/\kappa$ may become stable for certain injection strengths and frequency detunings while the period-1 solution destabilizes.

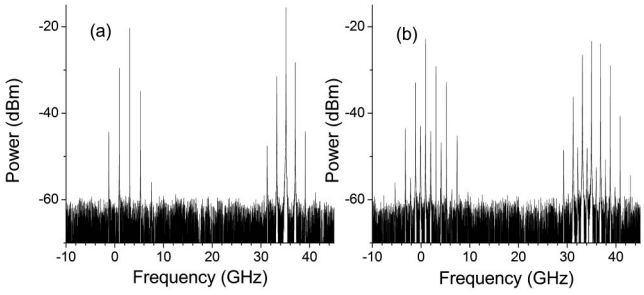

Fig. 6. Experimental optical spectra of the total output power when $\nu_i = 0.9$ GHz for different injected powers (a) $P_i = 7.5$ μW and (b) $P_i = 16.2$ μW.

We also show in Fig. 6 some representative examples of dynamics of PS. This figure shows how different types of periodic dynamics in both linear polarizations can be found for positive values of the frequency detuning: period-1 and period-2 dynamics are illustrated in Figs. 6(a) and 6(b), respectively.

In conclusion, we have investigated the PS of a single transverse mode VCSEL under parallel optical injection. We have found simultaneous injection locking of the parallel polarization mode and excitation of the free-running orthogonal polarization mode of the VCSEL. We have obtained very simple analytical expressions that describe both linear polarizations. Finally, we have done a linear stability analysis to find the conditions in which the unsupported mode is excited.

Funding. Ministerio de Economía y Competitividad (MINECO/FEDER) (TEC2015-65212-C3-1-P); Fonds Wetenschappelijk Onderzoek (FWO); Methusalem Foundation.

Acknowledgment. A. Quirce acknowledges FWO for her post doc fellowship and H. Thienpont and K. Panajotov are grateful to the Methusalem Foundation for financial support.

REFERENCES

1. A. A. Qader, Y. Hong, and K. A. Shore, IEEE J. Quantum Electron. **49**, 205 (2013).
2. K. Panajotov, I. Gatare, A. Valle, H. Thienpont, and M. Sciamanna, IEEE J. Quantum Electron. **45**, 1473 (2009).
3. Y. Hong, K. A. Shore, A. Larsson, M. Ghisoni, and J. Halonen, IEE Proc. Optoelectron. **148**, 31 (2001).
4. R. Lang, IEEE J. Quantum Electron. **18**, 6, 976 (1982).
5. G. H. M. van Tartwijk and D. Lenstra, Quantum Semiclass. Opt. **7**, 87 (1995).
6. S. Wieczorek, B. Krauskopf, T. Simpson, and D. Lenstra, Phys. Rep. **416**, 1 (2005).
7. M. Sciamanna and K. A. Shore, Nat. Photonics **9**, 151 (2015)
8. T. B. Simpson, J. M. Liu, A. Gavrielides, V. Kovanis, and P. M. Alsing, Phys. Rev. A **51**, 4181 (1995)
9. C. H. Chang, L. Chrostowski, and C. J. Chang-Hasnain, IEEE J. Sel. Top. Quantum Electron. **9**, 1386 (2003).
10. G. Friart, A. Gavrielides, and T. Erneux, Phys. Rev. E **91**, 042918 (2015).
11. A. Quirce, P. Pérez, H. Lin, A. Valle, L. Pesquera, K. Panajotov, and H. Thienpont, IEEE J. Quantum Electron. **50**, 921 (2014).
12. J. Martin-Regalado, F. Prati, M. San Miguel, and N. B. Abraham, IEEE J. Quantum Electron. **33**, 765 (1997).
13. P. Perez, A. Valle, and L. Pesquera, J. Opt. Soc. Am. B, **31**, 2574 (2014).
14. P. Perez, A. Quirce, A. Valle, A. Consoli, I. Noriega, L. Pesquera, and I. Esquivias, IEEE Photon. J. **7**, 1 (2015).
15. S. Osborne, K. Buckley, A. Amann, and S. O'Brien, Opt. Express **17**, 6293 (2009).